ARTICLE

BIOTECHNOLOGY and BIOENGINEERING

Marrow-Derived Stem Cell Motility in 3D Synthetic Scaffold Is Governed by Geometry Along With Adhesivity and Stiffness

Shelly R. Peyton,[1] Z. Ilke Kalcioglu,[2] Joshua C. Cohen,[3] Anne P. Runkle,[2] Krystyn J. Van Vliet,[1,2] Douglas A. Lauffenburger,[1,3,4,5] Linda G. Griffith[1,5,6]

[1]Department of Biological Engineering, Massachusetts Institute of Technology, Cambridge, Massachusetts 02139; telephone: 617-253-0013; fax: 617-253-2400; e-mail: griff@mit.edu

[2]Department of Materials Science and Engineering, Massachusetts Institute of Technology, Cambridge, Massachusetts

[3]Department of Chemical Engineering, Massachusetts Institute of Technology, Cambridge, Massachusetts

[4]Department of Biology, Massachusetts Institute of Technology, Cambridge, Massachusetts

[5]Center for Gynepathology Research, Massachusetts Institute of Technology, Cambridge, Massachusetts

[6]Department of Mechanical Engineering, Massachusetts Institute of Technology, Cambridge, Massachusetts

Received 23 September 2010; revision received 29 November 2010; accepted 2 December 2010

Published online ? ? ? ? in Wiley Online Library (wileyonlinelibrary.com). DOI 10.1002/bit.23027

ABSTRACT: Design of 3D scaffolds that can facilitate proper survival, proliferation, and differentiation of progenitor cells is a challenge for clinical applications involving large connective tissue defects. Cell migration within such scaffolds is a critical process governing tissue integration. Here, we examine effects of scaffold pore diameter, in concert with matrix stiffness and adhesivity, as independently tunable parameters that govern marrow-derived stem cell motility. We adopted an "inverse opal" processing technique to create synthetic scaffolds by crosslinking poly(ethylene glycol) at different densities (controlling matrix elastic moduli or stiffness) and small doses of a heterobifunctional monomer (controlling matrix adhesivity) around templating beads of different radii. As pore diameter was varied from 7 to 17 μm (i.e., from significantly smaller than the spherical cell diameter to approximately cell diameter), it displayed a profound effect on migration of these stem cells—including the degree to which motility was sensitive to changes in matrix stiffness and adhesivity. Surprisingly, the highest probability for substantive cell movement through pores was observed for an intermediate pore diameter, rather than the largest pore diameter, which exceeded cell diameter. The relationships between migration speed, displacement, and total path length were found to depend strongly on pore diameter. We attribute this dependence to convolution of pore diameter and void chamber diameter, yielding different geometric environments experienced by the cells within. Biotechnol. Bioeng.

Biotechnol. Bioeng. 2011;xxx: xxx–xxx.

KEYWORDS: mesenchymal stem cell; hydrogel scaffold; poly(ethylene oxide); migration

Correspondence to: L. G. Griffith

Contract grant sponsor: NIH/NIGMS Cell Migration Consortium
Contract grant number: GM064346
Contract grant sponsor: NIGMS NRSA Fellowship
Contract grant number: GM083472
Contract grant sponsor: NSF CAREER
Contract grant number: CBET-0644846
Additional Supporting Information may be found in the online version of this article.

Introduction

Connective tissue defects arising from genetic disorders, tumors, or trauma represent an ongoing challenge for surgical reconstruction (Kumagai et al., 2008; Shegarfi and Reikeras, 2009). Traditional approaches, including implantation of cadaver tissue, can provide functional repair, and newer strategies using porous scaffolds to guide colonization by endogenous progenitor cells are aimed at achieving regeneration (Healy and Guldberg, 2007). In such strategies, cells from sources such as marrow may be transplanted along with the scaffold, or the scaffold alone may attract cells from local tissue. Transplantation of either fresh or culture-expanded marrow-derived multi-potent stromal cells, or mesenchymal stem cells (MSCs), is involved in many

therapeutic strategies since they have the potential to differentiate down several connective tissue pathways (Friedenstein et al., 1966; Jiang et al., 2002; Pittenger et al., 1999; Sekiya et al., 2002). Successful regeneration requires scaffolds with mechanical stability, appropriate geometry, and appropriate biochemical and biophysical cues to drive cell infiltration, proliferation, and differentiation as the scaffold degrades. Biophysical cues from the scaffold may be important for this regenerative process, as it has been shown that mechanical stimuli (Chen and Hu, 2006; Simmons et al., 2003; Sumanasinghe et al., 2006), substratum stiffness (Engler et al., 2006; Maloney et al., in press), 3D porosity (Kasten et al., 2008), and the adhesive background (Kundu and Putnam, 2006; Lee et al., 2009; Martino et al., 2009) can potentially influence the differentiation trajectory of MSC populations. This motivates us to investigate how some of these biophysical factors may impact MSC migration, and therefore their ability to infiltrate a scaffold.

Cell motility is known to be strongly influenced by biophysical as well as biochemical properties of the extracellular matrix (Peyton et al., 2007). On two-dimensional model substrates, motility depends biphasically on both the cell-substratum adhesivity (Palecek et al., 1997) as well as substrata mechanical properties typically defined by elastic moduli (Peyton and Putnam, 2005). It has been hypothesized that this biphasic behavior arises due to a balance of cell-generated contractile forces against cell-substratum adhesion (Peyton and Putnam, 2005). Whether or not a similar relationship between motility and matrix biophysical cues is present in three-dimensional matrices is not yet clear. Although reports have shown that these biophysical aspects of matrices have an affect on cell migration (Zaman et al., 2005, 2006), it is not yet known if maximal cell motility in 3D still depends strongly on matrix adhesivity and stiffness, or if other features of the 3D migration environment dominate. Geometric effects associated with porosity, along with matrix degradation (Even-Ram and Yamada, 2005), which cause dramatic changes in migration-associated machinery (Cukierman et al., 2001), may be key factors governing the rate cells move through porous 3D matrices. However, porosity effects remain especially challenging to study systematically, in terms of both migration visualization and independent control of biophysical properties of the porous scaffold.

To examine how the interplay of 3D scaffold geometry with biochemical and biophysical properties of the matrix affect MSC migration, we have adapted a macroporous, three-dimensional synthetic extracellular matrix model system in which we can control porosity along with matrix stiffness and adhesivity. This system captures a range of biophysical properties exhibited by regenerative scaffolds described in the biomaterials literature, to determine how these separate factors may regulate progenitor cell migration in 3D. We show here that matrix adhesivity and stiffness influence MSC motility in this 3D matrix. Interestingly, however, geometry appears to be the dominating biophysical cue in a manner that is not intuitive: scaffold geometry and molecular matrix properties work together to govern migration in ways that are not obvious by considering either factor individually. These findings are relevant for analysis of basic physiological processes of cell migration, such as migration of MSCs through heterogeneous tissues, as well as for the design of scaffolds that promote efficient dispersion of cells throughout.

Materials and Methods

Cell Culture

hTERT MSCs (immortalized marrow-derived, or "mesenchymal," stem cells, a generous gift from Dr. Junya Toguchida (Okamoto et al., 2002)) were routinely cultured in Dulbecco's modified eagle's medium (DMEM), supplemented with 1% L-glutamine, 1% penicillin–streptomycin, 10% fetal bovine serum (Gemini Bio-Products, West Sacramento, CA), 1% non-essential amino acids, and 1% sodium pyruvate (all from Invitrogen, Carlsbad, CA). Cells between passages 12–35 were used for all experiments. To measure cell diameters, MSCs were first treated with a live-cell fluorescent dye (CMFDA, Invitrogen) according to the manufacturer's instructions. Cells were trypsinized, visualized via confocal microscopy, and the cell spherical diameters were measured with Imaris ($N = 113$). The differentiation capability of this particular MSC line has been characterized elsewhere (Kobune et al., 2003).

Poly(Ethylene Glycol) Scaffold Fabrication

Three-dimensional (3D) scaffolds based on poly(ethylene glycol) (PEG) were fabricated by adapting a previously published system (Stachowiak and Irvine, 2008). PEG-dimethacrylate (PEGDMA, average Mn 750, 14-15-mer, Sigma–Aldrich, St. Louis, MO) and PEG-methacrylate (PEGMA, average Mn 526, 10-11-mer, Sigma-Aldrich Chemical Company, St. Louis, MO) were combined in various ratios (10–34% v/v PEGDMA/reaction solvent) with 0.05–0.6% v/v (PEGMA/reaction solvent) for ligand addition with 0.8% w/v 1-hydroxy-cyclohexylphenyl ketone initiator (Sigma) and buffered with 3:1 PBS/EtOH. For pore size analysis and migration experiments, 5 mM (0.05% v/v of reaction solution) of fluorescein-o-methacrylate (Sigma) was included to visualize the scaffolds.

Monodisperse poly(methyl methacrylate) microspheres (PMMA, Sigma) with nominal diameters of 20, 30, 40, 50, or 60 μm were concentrated to 65% (w/v) in 70% EtOH and pipetted into circular PDMS gaskets (6 mm × 1 mm, EMSdiasum, Hatfield, PA) adhered to Sigmacote-pretreated glass slides. The microspheres were shaken vigorously on an orbital shaker (350 rpm) until dry (4 h). Twelve microliters of the polymer solution was then added to the dried bead cake and photopolymerized via UV-light irradiation (3 min at 365 nm). Scaffolds were soaked for 3 days in

tetrahydrofuran (THF) with regular solvent changes to leach away the PMMA templating beads and leave behind a macroporous PEG hydrogel. Two-dimensional (2D) hydrogels were made using the same PEGMA and PEGDMA formulations to compare with 3D results; polymer solutions were polymerized between glass plates separated by thin (180 μm) Teflon spacers, similar to previous studies (Peyton and Putnam, 2005). The resulting 2D hydrogels were soaked for 1 h in THF to remove any unreacted monomers then reacted with adhesive ligand according to the same protocol for 3D scaffolds.

Ligand Attachment to Hydrogel Scaffolds

Macroporous PEG scaffolds were synthesized with PEGMA added in proportions to yield 1–12.5 mM free hydroxyl groups in the final gel. Gels were reacted for 1 h at room temperature with nitrophenyl-chloroformate (NPC, Sigma) in 100-fold molar excess to the hydroxyl groups in PEG-methacrylate (Tugulu et al., 2005). The reaction was quenched and scaffolds were washed 4× in THF. For ligand attachment, two-fold molar excess of G*RGD*SP (integrin-binding sequence underlined, Anaspec, Fremont, CA) was added to the gels, and incubated overnight at room temperature, protected from light, in dimethylformamide (Tugulu et al., 2007). Prior to use in cellular experiments, scaffolds were washed 4× in THF and then 2× in PBS. They were sterilized by exposure to UV-light in the tissue culture hood for 1 h while in PBS. To quantify the relative extent of reaction of the peptide, TAMRA-lysine was used in place of G*RGD*SP at a 1:25 molar dilution from the available NPC groups since the maximum readable concentration range of TAMRA in the fluorescent plate reader was 2.5 mM.

Scaffold Microstructural and Mechanical Properties

Macroporous gels were examined qualitatively by scanning electron microscopy (SEM) and quantitatively via confocal microscopy. For SEM imaging, macroporous hydrogels were made as described above, allowed to fully swell in PBS, replaced with water, then flash-frozen in liquid nitrogen and lyophilized. Dried gels were gold/paladium sputtered for 2 min and imaged on a JEOL scanning electron microscope ($V = 5$ kV, w.d. = 20 mm). Hydrogels polymerized in the presence of 5 mM fluorescein-o-methacrylate were allowed to fully swell in PBS, then imaged on an LSM 510 line-scanning confocal microscope to visualize and measure both the diameter of the void chambers and the interconnecting pores throughout the gel ($N = 27$–28 for each condition).

Instrumented indentation on fully hydrated, immersed macroporous hydrogels was conducted via a pendulum-based instrumented nanoindenter (NanoTest, Micro Materials Ltd, Wrexham, UK) with a force resolution of 1 μN and a displacement resolution of 0.1 nm. Hydrogels made from PMMA bead diameters of 20, 40, and 60 μm and PEGDMA crosslinker contents of 10%, 17%, and 34% (v/v) were tested. Additionally, nonporous PEGDMA gels with similar dimensions and crosslinker content were prepared and tested in order to directly quantify the elastic properties of the hydrogel solid phase, and to compare the results with predictions of macroscopic elastic moduli for the Gibson–Ashby cellular solid model (Gibson and Ashby, 1999; Harley et al., 2007). This model correlates Young's modulus of the solid of which the foam is comprised, E_s, to the Young's modulus of the elastomeric, open-celled foam, E^*, according to the relation:

$$E^* = C[\rho^*/\rho_s]^n E_s \quad (1)$$

where C is a constant of proportionality related to void geometry and is ~1 for open-cell foams, ρ^*/ρ_s is the relative foam density and is 0.26 for this study assuming an ideal packing density of the templating beads according to the Kepler conjecture, and n is an exponent that defines whether the dominant mechanism of deformation is bending or axial stretching (Jain et al., 2001). Hydrogels were adhered to a glass slide with a thin layer of cyanoacrylate-based adhesive and mounted on an aluminum support. All experiments were conducted with the sample fully immersed in PBS using a modified platform for in situ liquid experiments (Constantinides et al., 2008). Samples were indented with a spherical ruby indenter of radius $R = 1$ mm, ($n = 9$ locations for each hydrogel sample), with loading, dwell, and unloading times of 10 s, 30 s, and 10 s, respectively. A maximum depth of 20 μm was chosen to contact as many pores as possible. The elastic modulus inferred from indentation, E_i, (equivalent to E^* of porous gels and E_s of nonporous gels) was calculated via analysis of the unloading response according to the method of Oliver and Pharr (1992).

The mesh size, ξ, for these hydrogels as a function of crosslinker content was determined according to the method initially described by Flory (1953) and modified by Canal and Peppas (1989):

$$\xi = \upsilon_{2,s}^{-1/3}(\bar{r}^2)^{1/2} \quad (2)$$

where $\upsilon_{2,s}$ is the swollen volume fraction of the polymer and $\bar{r}^2$ is the end-to-end distance of the PEG. Porous and nonporous hydrogels of the same bulk diameter and height were made as previously described and weighed both at their fully swollen state (in PBS) and in their completely dried state (via lyophilization).

Cell Migration Analysis

For migration experiments in 3D scaffolds, CMFDA-treated MSCs were concentrated to 5×10^5 cells/mL, and 20 μL of cell suspension (two separate cell loadings of 10 μL each) was loaded into each gel with light centrifugation (3 min, 700 rpm) to improve seeding efficiency (Roh et al., 2007). Cells were allowed to incubate and penetrate into the

scaffolds for 24 h before microscopy commenced. For 2D migration experiments, CMFDA-treated MSCs were seeded onto the surfaces of hydrogels at a concentration of 5–10×10^4 cells/gel. Medium was changed 4 h before every migration experiment to ensure consistency of growth factor stimulation. Cell motility was observed with either a PerkinElmer RS-3 confocal microscope or a Zeiss AxioObserver equipped with a CARVII spinning disk and EXFO light source at 15 min intervals of 150 μm *z*-stacks with 3–5 μm spacing over 12 h in a temperature and CO_2-controlled humidified chamber. No *z*-stacks were generated for 2D migration analysis. Cell centroids were tracked using Imaris software (Bitplane, St. Paul, MN). Cells that migrated out of the field of view, underwent division, or had visual blebbing were noted (less than 1% of all cells appeared apoptotic) but not tracked (~5–10% of all cells within the field of view were not tracked due to these reasons). Average individual cell speeds were calculated from the individual cell tracks by measuring the distance traveled over each 15 min time interval and averaging these interval speeds over the entire 12 h time period. These average speeds for each cell were then averaged at each condition to generate mean cell speeds. Net displacement for each cell was calculated by subtracting the initial cell position (x, y, z) from the final cell position (x, y, z) at the end of 12 h. The "jump" number for each cell was determined by watching the migration behavior of each individual cell and counting the number of times each cell moved between two different void chambers.

Statistical Analysis

Statistical analysis was performed using Graphpad's Prism v5.0a and InStat v3.1a for Macintosh. Data are reported as mean ± standard error. *P*-Values less than 0.05 denote statistical significance according to a one-way analysis of variance (ANOVA) followed by a Student-Newman–Keuls post-test between multiple sets of data or a Bonferroni post-test between pairs of columns, unless otherwise noted.

Results

"Inverse Opal" Hydrogels Permit Tunable Porosity, Elasticity, and Adhesivity of 3D Scaffold

Using a sphere-templating approach, we created macroporous hydrogel scaffolds with tunable pore size, stiffness, and adhesive peptide levels (Fig. 1). We adapted an inverse-opal processing technique, which uses leachable PMMA microspheres to create an ordered, porous scaffold comprising spherical "void chambers" connected by pores (da Silva et al., 2010; Marshall and Ratner, 2005; Stachowiak et al., 2005). By varying the diameter of the templating beads from 20 to 60 μm, we achieved pore sizes ranging from 7 to 17 μm (measured in the hydrated state via confocal microscopy), independent of PEG crosslinker content. These pore sizes were selected to span a range from dimensions much smaller than the relaxed spherical cell diameter (measured as 16 ± 3μm, similar to previous reports of MSC size (Jing et al., 2008)) to a dimension comparable to the mean spherical cell diameter. Cells were initially seeded into void chambers, which are the same diameter as the PMMA templating bead (shown by a black arrow in the SEM inset), and were then allowed to move between void chambers through the pores, where two PMMA beads were initially in contact during templating (white arrow). Ten or more SEM micrographs per condition were used to determine that the gel's honeycomb structure approached this theoretical limit of 12 pores per void chamber (average of 9–10 pores per chamber) for all conditions studied (data not shown).

We found that elastic moduli increased with increasing volume percent of PEDGMA crosslinker (Fig. 1B), for both nonporous gels and porous hydrogels of identical composition for bead diameters of 20, 40, and 60 μm. E^* of these porous scaffolds varied from 3 to 100 kPa for an increase in crosslinker from 10% to 34% v/v PEGDMA. As expected, microscale porosity reduced the stiffness as a function of crosslinker as compared to the nonporous versions of these same gels ($56\,\text{kPa} < E_s < 7\,\text{MPa}$). Elastic moduli of the nonporous samples E_s represent the mechanical stiffness of the hydrogel material comprising the solid pore walls and struts of the porous samples. As the cells adhere directly to and migrate along these pore walls and struts, it is the mechanical stiffness of those regions—as opposed to E^* of the macroscopic porous hydrogel—that is expected to chiefly define the local mechanical environment of cells within the porous hydrogels. Variation of E_s over this kPa-to MPa-range for other substrata materials has been shown to affect cell behavior in other studies (Ochsner et al., 2010; Smith et al., 2010; Thompson et al., 2005). However, we note that this effective, local stiffness in our porous hydrogels is defined ultimately by both the material stiffness E_s, as well as the structural stiffness described by relative dimensions and boundary conditions of those pore walls and struts.

Despite this difference between macroscopic gel stiffness and the local effective mechanical environment of the adherent cell, quantification of the E^* for these porous hydrogels (Fig. 1B) is useful in that it allows comparison of elastic properties as commonly reported for tissues and other types of engineered scaffolds, when measured via micro- to macroscopic mechanical methods. The microscale-porous gels of 10% v/v PEGDMA were too compliant to be tested experimentally using instrumented indentation; the topology of these gels also prohibited atomic force microsopy-enabled indentation. For these porous 10% v/v PEGDMA gels, E^* was instead predicted by use of a validated Gibson and Ashby (1999) model. This was achieved by measuring E_s for all nonporous gels and E^* for the 17% and 34% v/v PEGDMA porous gels; these measured E_s and E^* for the stiffer porous gels were used to obtain n (the model mode of strut deformation in Eq. 1). This model, with now validated values of n for each pore diameter, $C \sim 1$ and

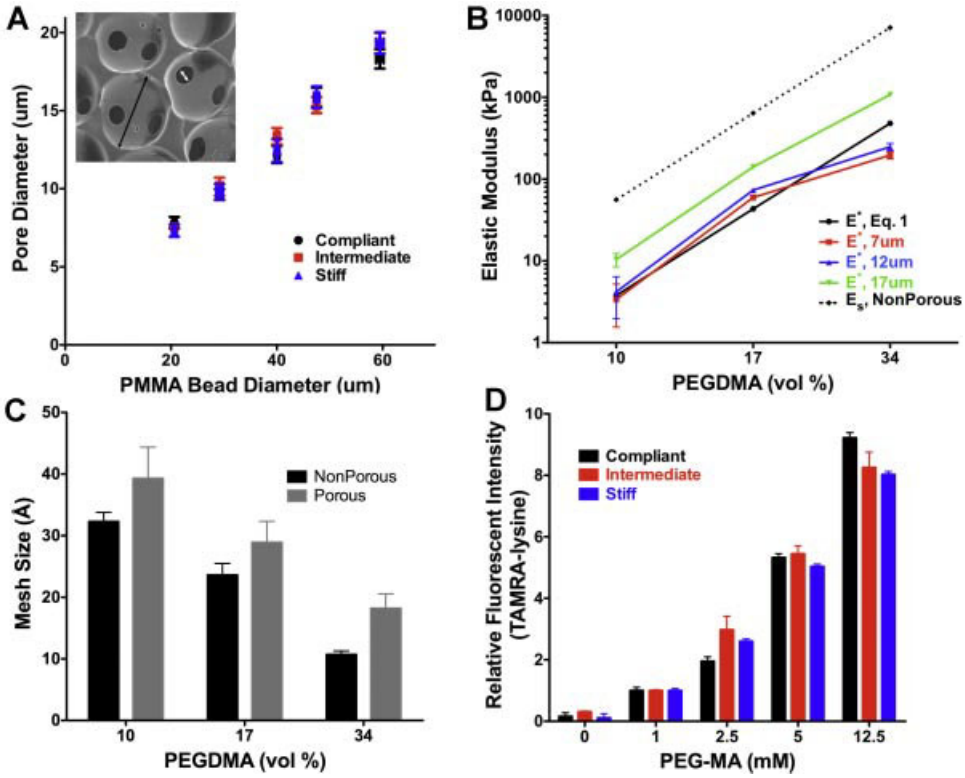

Figure 1. PEG-based synthetic matrices have independently tunable porosity, elastic moduli, and adhesivity. **A**: By changing the diameter of the leachable PMMA beads from 20 to 60 μm (*x*-axis), the pore sizes between void chambers (measured using confocal microscopy on hydrated samples) can be tuned from 7 to 17 μm in diameter (*y*-axis). This process is independent of changing the PEGDMA crosslinker content to create compliant (10% v/v PEGDMA, 56 kPa, black circles), intermediate (17% v/v PEGDMA, 640 kPa, red squares), or stiff (34% v/v PEGDMA, 7 MPa, blue triangles) hydrogels. When comparing between bead diameters, pore sizes are all statistically different from each other, regardless of stiffness ($P \leq 0.05$, SEM shown for 27–30 pores measured for each condition). A representative SEM micrograph (inset) shows the void chamber diameter (the original diameter of the PMMA bead, black arrow) in contrast to the pore diameters (where two beads were originally in contact, white arrow) for a representative gel with a 20 μm void chamber diameter and 7 μm pore diameter. **B**: The elastic modulus for fully hydrated porous gels with pore sizes of 7, 12, or 17 μm follows the predictive model (solid black) described by Gibson and Ashby (1999) based on the elastic modulus of the solid, represented by nonporous gels (E_s, dashed black). Errors are SEM for three separate samples with nine locations per sample. **C**: The mesh sizes of these gels depend on the crosslinker content (*x*-axis) but not on whether gels are porous (gray bars) or nonporous (black bars). Comparisons of mesh sizes between crosslinker contents was significant in all cases ($P < 0.001$), but the difference in mesh size between porous and nonporous conditions was not significant, regardless of crosslinker content. **D**: Using a fluorescent reporter substitute for the adhesive ligand (G*RGD*SP) shows that the bulk concentration of peptide can be controlled via the initial PEGMA concentration ($P < 0.05$), but is independent of crosslinker content (comparisons between compliant, intermediate, or stiff gels not significant).

relative density $\rho^*/\rho_s = 0.26$, was then used to estimate E^* of the 10% v/v porous gels. Although the model predicts that the macroscale elastic modulus is independent of pore diameter, we observed that E^* was greatest for the porous gels of largest diameter (17 μm) for all %v/v PEGDMA. These deviations are reasonably attributed to the neglect of poroelastic contributions in the "dry" cellular solid model of Gibson–Ashby, and other studies adopting the Gibson–Ashby model for open-cell foams have also reported this phenomenon (Stachowiak et al., 2005). We also found that the inclusion of the templating beads did not affect the swelling (mesh size) of the hydrogels, by comparing porous and nonporous matrices (Fig. 1C).

We estimated the concentration of covalently linked G*RGD*SP present in the final gels using a reaction with a fluorescent reporter (TAMRA-conjugated lysine) of similar chemical structure and molecular weight to validate that the peptide linkage varied in a monotonic fashion with the concentration of peptide in the reaction solution (Fig. 1D). Using this technique, we observed that the extent of reaction appeared independent of crosslinker content in the gels.

Displacement of Cells Into Scaffolds Is Not Maximized With Higher Pore Diameters

To design scaffolds appropriate for regeneration, the most important aspect of this study was to determine which of the biophysical properties we varied produced a heightened ability of these progenitor cells to migrate into and infiltrate the model scaffold. We initially hypothesized that the net displacement of cells in these macroporous scaffolds would increase with increasing pore diameters, since increasing pore diameter would ostensibly allow for increasing freedom of cell motility. However, this initially intuitive, *a priori* prediction was not borne out in all the conditions tested. In

the smallest pore diameters (7 μm pores and 20 μm void chambers), the ability of cells to displace into the scaffold over the course of the 12 h observation was minimal. In fact, only a few outlier cells appeared to move more than 50 μm away from their starting point, regardless of matrix stiffness or adhesive ligand concentration (Fig. 2A). Surprisingly, the condition that maximized cell displacement was found in scaffolds with a 12 μm pore diameter at the stiffest and most adhesive conditions used in this study (Fig. 2B), and not in the larger and presumably non-restrictive 17 μm pore diameter (Fig. 2C). However, given that cell spherical diameter was measured to be just 16 μm, it could be assumed that neither the 12 μm nor 17 μm pore diameters were necessarily restrictive to cell movement, and perhaps the geometries of these matrices are regulating cell displacement by another less obvious mechanism.

Migration Speed Is Influenced by Pore Size, Matrix Stiffness, and Adhesivity

To quantify how MSCs move through these 3D macroporous scaffolds and are able to generate the previous displacement phenomena, we analyzed cell migration speed as a function of the key biophysical parameters. Pore diameter in these 3D macroporous gels appears to have a pronounced effect on cell migration through the gel, further modulated by adhesivity and elasticity (Fig. 3). In the smallest pore diameters tested (7 μm, Fig. 3A), the average cell speed does not appear to be affected by matrix stiffness (black, red, or blue lines) or the bulk concentration of G*RGD*SP (*x*-axis). In fact, cell speed in this case approaches the level we measured to be migration "noise" (i.e., small centroid movements of cells trapped in a void chamber in the smallest pore diameter condition). A majority of cells in these conditions appeared to be "trapped" and were not able to generate any intrachamber motility, leading to universally low cells speeds (Fig. 3D and Suppl. Movie 1). Similarly, for the intermediate pore diameter condition (12 μm, Fig. 3B), variations in matrix stiffness and adhesivity exert little effect on cell migration speed; however, cell speeds across all these conditions are higher than for cells in the 7 μm pore diameter case. This shift to higher cell speeds with larger pore diameters could be due to intrachamber motility, as the corresponding void chamber dimension approaches more than twice that of the spherical cell diameter, or increased interchamber motility resulting from the increase in the interconnected pore diameters (Fig. 3E).

Finally, in the largest pore diameters tested here (17 μm, Fig. 3C and F), interesting trends in motility emerge as a function of matrix elastic properties and adhesivity. We observed two "peaks" in migration speed for this pore size: one at an intermediate material stiffness and intermediate concentration of adhesive ligand, and another at the most stiff and most adhesive condition. This apparent rightward shift to more adhesive environments when the gel is stiffened is reminiscent of previous observations of tumor cell migration behavior in 3D matrices constructed by systematic variation of Matrigel® properties (Zaman et al., 2006). There was no apparent dependence of cell speed on RGD density or matrix stiffness in the intermediate pore diameter condition, yet these parameters did affect displacement. The condition allowing for highest cell displacement in hydrogels with pore diameter of 12 μm did not relate to the

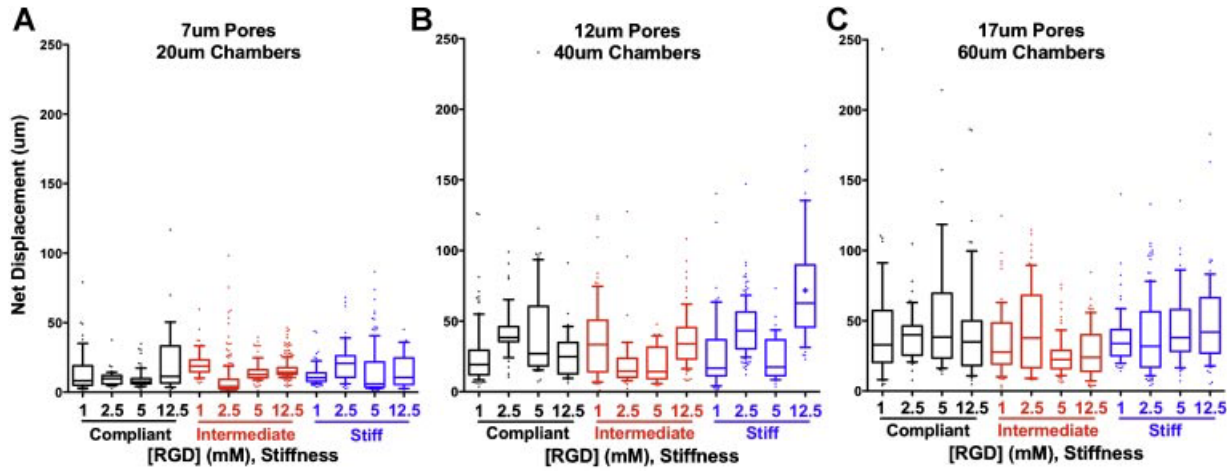

Figure 2. Net displacement of cells migrating in scaffolds is highest in an intermediate pore diameter condition. Subparts (**A**–**C**) are box and whisker plots where most outliers are shown (a negligible number of outliers over top of *y*-axis limits cut off for better data visibility), the whiskers range from 10% to 90%, and the horizontal bars are medians (means of conditions with significance given as "+"). A: In the smallest pore diameter case, displacement is minimal, and only outliers are able to reach over 50 μm away from their starting point over the 12-h experiment. B: The most net displacement in the intermediate diameter pore condition occurs at the stiffest gel and highest concentration of RGD tested ($P \leq 0.0001$ compared to every other data point). C: In the largest pore size case, displacements are similar to those seen in the intermediate pore diameter case, and neither matrix stiffness nor adhesivity significantly affects displacement.

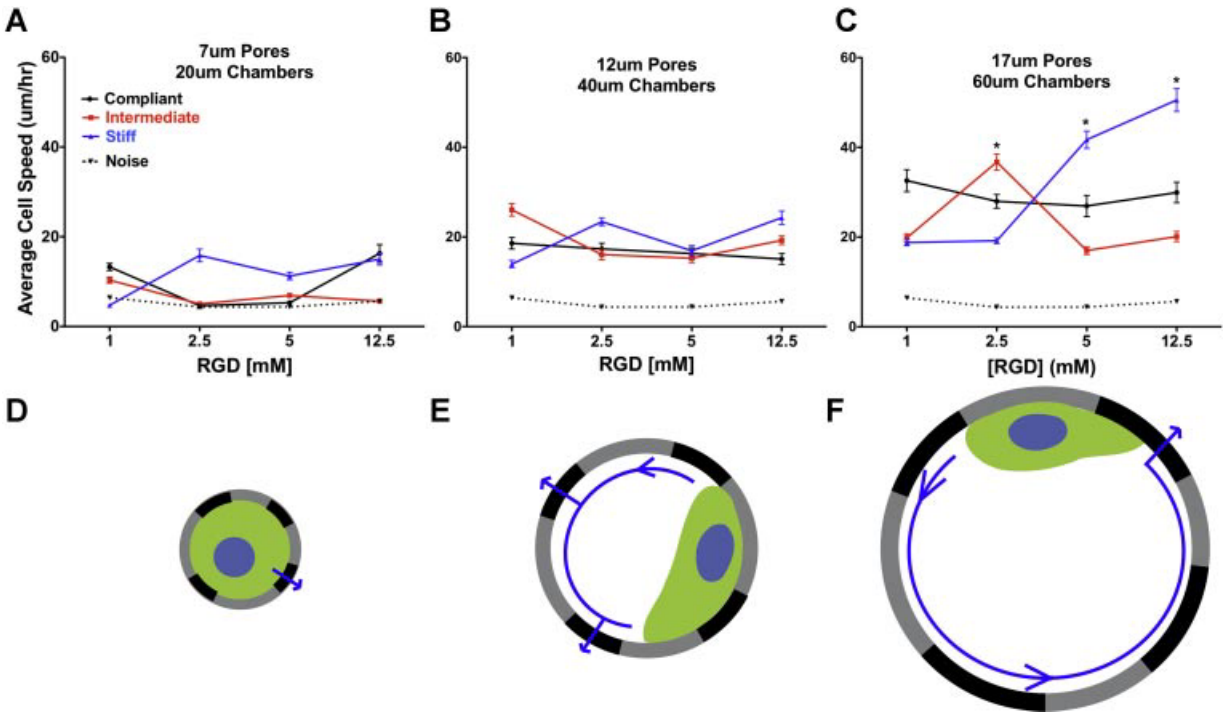

Figure 3. Changes in adhesivity and elastic moduli have the most pronounced impact on cell migration in the largest pore sizes. **A** and **D**: In the smallest pore diameter condition, cell speed is most often the same as the "noise" level, which is the speed of cells in the smallest void chambers that never migrate from their starting position. **B** and **E**: In the intermediate diameter pores, cell speed still appears to have minimal dependence on the levels of adhesion and stiffness; however, cell speed is qualitatively increased from the smallest pore size case, presumably due to room for intrachamber movement. **C** and **F**: In the largest pores, a dependence on adhesivity and elastic moduli emerges. The following points are statistically significant from all other data points: intermediate stiffness gel with 2.5 mM RGD, and stiff gels with 5 and 12.5 mM RGD ($P \leq 0.05$).

highest cell speeds observed. However, this condition of highest cell displacement did correspond to the condition allowing for maximum interchamber mobility (Suppl. Fig. 3). This maximized interchamber movement at the stiffest, most adhesive hydrogel condition could be due to the fact that cell–matrix traction will be greatest under such conditions. These high tractional forces may be necessary for interchamber movement, since at chamber connections, hydrogel material comes to a point and cells must pull themselves over a topographically steep surface to reach into the adjacent chamber. Further, a recent modeling effort has discovered that cytoskeletal tension is inhibited at higher substrate curvatures (Sanz-Herrera et al., 2009). That theoretical study is consistent with our observation that cells in the 40 μm void chambers require a substratum lending to maximum traction forces to achieve maximum displacement.

We investigated MSC motility on 2D substrates with the same stiffness and adhesive conditions examined in the 3D scaffolds to isolate these parameters from the geometric effects. We were unable to discern a strong dependence of migration speed on stiffness or adhesion on the 2D substrates tested here (Suppl. Fig. 1). This could be due to the fact that others have reported a biphasic motility dependence on adhesivity and stiffness in the presence of full-length matrix proteins, such as fibronectin and collagen (Palecek et al., 1997; Peyton and Putnam, 2005). Here, we have used the short peptide sequence G*RGD*SP, which binds to $\alpha_v\beta_3$ with high affinity, yet does not engage the $\alpha_5\beta_1$ nearly as effectively; $\alpha_5\beta_1$ engages with the synergy sequence inherent to fibronectin, which may be required for this biphasic dependence. In a previous study comparing the motility of fibroblasts on either substrates with RGD clusters or fibronectin, only the full-length protein condition was able to stimulate this biphasic dependence (Maheshwari et al., 1999, 2000). Current evidence from our lab has also shown that this specific MSC cell line exhibits a biphasic migration behavior in the presence of fibronectin, but not the $\alpha_v\beta_3$ binding protein vitronectin (publication *in preparation*). Further, our 2D gels are substantially stiffer (our "compliant" nonporous hydrogel exhibits an elastic modulus of approximately 60 kPa) than those substrates used by others who have observed this biphasic behavior (Fig. 1B). We chose these much stiffer PEG hydrogel conditions for our studies due to the relevance for scaffolds generally used in bone regeneration applications. Interestingly, just as in the case of the largest pore diameters, conditions lending to high migration speed also lend to long path lengths, but not high displacements (Suppl. Fig. 1). This suggests that the largest pore diameters considered here, comparable to the cell diameter, represent an approximate 2D surface for migration wherein the stiffness

of the nonporous span (E_s) and the length scale dimensions of this span are the more relevant, defining characteristics of the mechanical microenvironment.

Migration Efficiency Is Dictated by Scaffold Geometry

Interestingly, these trends for cell speeds found as a function of these varying scaffold properties were not sufficient to explain the displacement behavior found in Figure 2. Maximum displacement was seen in the 12 μm pore diameter condition in stiff matrices and a maximum adhesive ligand concentration. However, this condition did not generate maximum cell speeds, which were found in large pore diameters at varying adhesive and stiffness conditions. Therefore, there appears to be a surprising convolution of geometric properties of the scaffold as pore diameter is varied, with matrix stiffness and adhesivity cues maintained constant. To examine this, we analyzed how well cells were able to translate cell speeds into functional displacement into the scaffolds by assigning a migration efficiency index, which we defined as the ratio of the net displacement (Fig. 2) to the total path length (Suppl. Fig. 2). This parameter is conceptually analogous to previous measurements of "chemotactic index" present under conditions of attractant gradients (which are absent in this study). A maximum migration efficiency of 1.0 is defined here as a perfect translation of a cell's path length into displacement into the scaffold, whereas a migration efficiency is zero for a perfectly random walk.

In Figure 4A, the condition which generated maximum cell displacements into the scaffold (Fig. 2B) also had the highest migration efficiency index for the pore diameters tested here, even though maximum efficiency index did not coincide with maximum cell speeds (Fig. 3B). Interestingly, those conditions in the largest pore diameters that gave rise to highest cell speeds (Fig. 3C) had the lowest migration efficiencies. This inverse correlation implies that cells are traveling quickly within large void chambers, yet not moving through presumably non-restrictive pores (Fig. 3F). Expectedly, we saw the highest migration efficiencies in the 2D case (Fig. 4C), where there were no geometric restrictions to cell movement (note the presence of cells with efficiency indices approaching 1.0).

Cells "Jump" Most Often Through Intermediate Pore Diameters

To relate how these changes in pore diameters were able to generate such distinct cell migration speed, efficiency, and displacement behaviors, we quantified the extent to which pore diameter regulated the ability of cells to move between void chambers via pores. Each instance a cell moved through a pore into a new void chamber it was counted as a "jump". Given that we previously observed the highest cell speeds in the largest pore diameter conditions (Fig. 3C), we hypothesized that the displacement of cells into the scaffolds would increase with higher pore sizes and with the number of instances cells moved through pores. Not surprisingly, displacement increased for each pore diameter with an increasing number of jumps taken (Fig. 5A). However, there was no appreciable difference when comparing the medians of cell populations that jumped more than once between the intermediate and large pore diameters, supporting the previous observation of maximum displacement in an

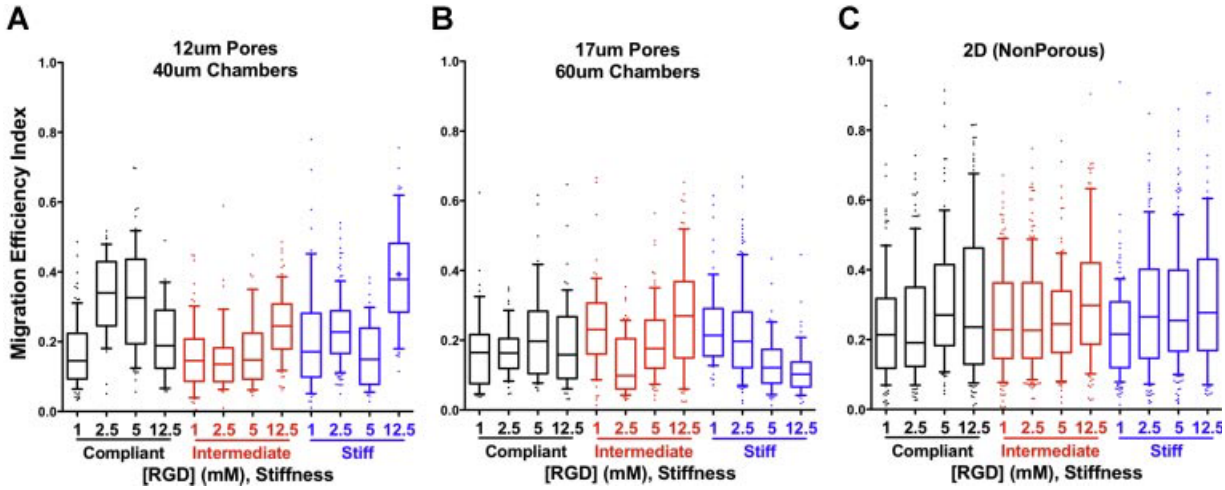

Figure 4. Migration efficiency is dictated by scaffold geometry. **A**: Migration efficiency (the ratio of net displacement to total migration path length) was highest at an intermediate pore diameter at the stiffest and most adhesive condition ($P \leq 0.001$ higher than all other intermediate and large pore diameter conditions). **B**: Migration was less efficient in the largest pore diameter condition. Those conditions leading to least efficient migration also exhibited highest cell speeds (intermediate stiffness at 2.5 mM RGD, stiff at 5 and 12.5 mM RGD, $P \leq 0.05$ lower efficiency than all other 17 μm points). **C**: Overall, the highest migration efficiencies in the 2D case, where there were no geometric restrictions to cell movement.

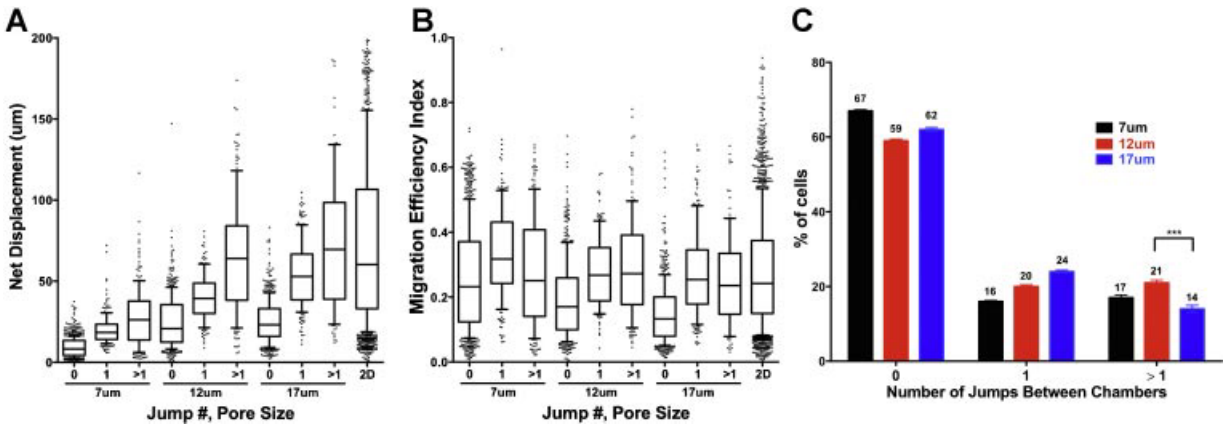

Figure 5. The likelihood of cells to jump is highest in intermediate pore diameters. **A**: Within each pore diameter group, cell displacement increases with the number of jumps a cell takes; however, there is no qualitative difference between the displacement of cells that take more than 1 jump in the 12 and 17 μm cases (whiskers: 10–90%, bars: medians). The displacement of cells on 2D surfaces is shown as a reference. **B**: Migration efficiency index is highest for cells undergoing more than one jump in the intermediate pore diameter condition ($P \leq 0.0001$ higher than the largest pore diameter condition). The migration efficiency of cells on 2D gel surfaces is shown as a reference. **C**: Histogram describing population of cells making 0, 1, or more than 1 jump, grouped by pore diameter. The probability distribution that cells will jump more than once is lowest in the 17 μm pore size, even though pore sizes here are not restrictive. The percentage of cell population for each jump number is indicated above corresponding bars. Error bars are SE and were generated by averaging each individual stiffness and RGD concentration condition. Asterisks indicate a statistically significant difference when comparing cells jumping more than once in 12 and 17 μm pore diameters ($P < 0.0001$).

intermediate pore diameter case (Fig. 2B). To help explain this, we analyzed the migration efficiency (Fig. 5B) for these groups as well as counted the number of instances that cells jumped with respect to the scaffold pore diameter and observed that cells in scaffolds with intermediate pore diameters had a higher probability to jump more than once than in the larger pore diameter (Fig. 5C). Migration efficiency was statistically highest for cells taking more than one jump in the intermediate pore diameter condition. Interestingly, in the 7 μm pore diameter condition, efficiency was higher in instances of one jump than for cells taking more than one jump, suggesting that cells are moving back toward their initial position, or perhaps leaving protrusions in their initial chambers and returning there.

Scaffold Porosity Defines Geometric Microenvironment

To help explain these observed motility phenotypes, we investigated the relationship between cell diameter, void chamber diameter, and pore diameter and the resulting geometrical microenvironment cells might be experiencing in these macroporous scaffolds (Fig. 3E and F and Fig. 6). First, we used a theoretical packing density assumption to measure the arc lengths between pore edges, L_1:

$$L_1 = \frac{(2\pi r_v)}{6} - 2\left(\frac{1}{2d_p}\right) \quad (3)$$

where r_v is the radius of the void chamber and d_p is the diameter of a pore. For pores around the perimeter of a void chamber, the arc length between pore edges is 14.4 μm for a 60 μm chamber and 8.9 μm for a 12 μm chamber (L_1). Assuming ideal close packing of the templating spheres, pores form equilateral triangles throughout the void chamber sphere, and distances between pores is consistent everywhere. Further, we hypothesized that since the void chambers were of different diameters, cells may spread to a different extent while exhibiting this hamster-wheeling motility behavior in different chambers. Due to the increase

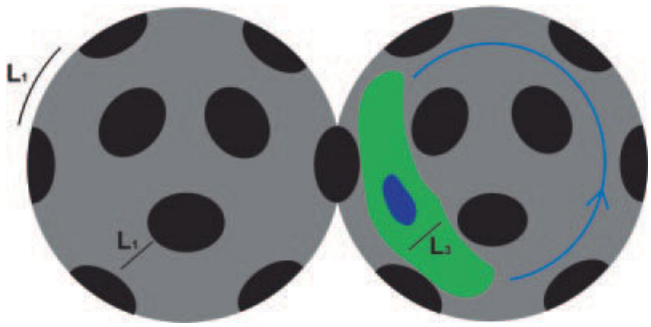

Figure 6. Hypothetical geometric relationships between cell and scaffold dictate migratory phenotypes in 3D porous matrices. Illustration shows theoretical distribution of pores in maximum close packing. In close packed spheres, the void chamber diameter (40 or 60 μm) and pore diameter (12 or 17 μm) combine to give a defined arc length (L_1), which is consistent between all available pores. Relationship between the average cell width of cells in spinning in void chambers L_3, and the distance between pore edges (L_1) regulate the cell's geometric environment, and therefore a cell's propensity to jump between chambers, its speed, path length, and displacement. Blue line represents an observed migratory phenotype cells often take within void chambers, possibly avoiding pores. In the 12 μm pore size condition (40 μm void chamber), the average cell width is 1.1 times the average distance between pore edges, allowing for both intrachamber and interchamber motility. In the largest pore size condition (60 μm void chamber, 17 μm pore), the average cell width is 70% the arc length between pore edges, leading to increased intrachamber motility.

in void chamber diameter, average cell lengths increased from 27.8 to 39.7 μm between the 40 and 60 μm void chambers, and as a result, average cell widths (L_3) decreased slightly from 9.8 to 9.5 μm. More importantly, however, the dimensionality ratio between the average cell width to the average available material space between pores (L_3/L_1) decreased from 1.1 to 0.7 when comparing cells within a 40 μm void chamber (12 μm pores) to a 60 μm void chamber (17 μm pores). Functionally, this means that cells within the larger void chambers, on average, are able to migrate on material "tracks" that are 30% larger than the cell widths, which may help explain the tendency for intrachamber motility, even though pores are quite large. Such quantification may also help explain why cells in the smaller void chambers migrate between chambers most often, given that they are much more likely to be immediately in contact with available pores (Suppl. Mov. 4).

Assuming ideal hexagonal or face-centered closed packing of the templating beads, pore edges are theoretically 14.4 μm apart (Fig. 6), and, given the motility speeds we measured, cells encounter a pore edge more than once per hour. A lack of jumping could be explained by less than ideal packing of the templating beads and, as a result, the presence of chambers with no interconnecting pores. However, SEM analysis showed that the absence of pores can only account for 6% of total chambers, and we observed nearly 60% of cells to undergo zero jumps over the time course in all pore diameter conditions (Fig. 5C). Instead, it appears that cells encounter many pores during fast intrachamber movement, yet do not appear to move through available pores. We also observed a substantial population of cells with the ability to move between chambers in the smallest pore diameter condition, which we attribute to heterogeneities within the cell line (where cell diameters ranged from 9 to 24 μm).

In the smallest pore diameters (7 μm, Fig. 3D), the cell diameter approaches the diameter of the enclosing void chamber. In this case, cells are always in contact with pores, yet pores must be small enough to be restrictive to movement (the 7 μm diameter of the pores is only about half the diameter of the cell (16 μm)), as we observed while watching motile cells in these scaffolds (Suppl. Mov. 1). In such cases, motility is dominated by intrachamber movement. This explains both why we see low motility and displacement in this condition, as well as why motility does not appear to depend on either matrix elastic moduli or adhesivity. We observed a wide range of cell spherical diameters, and most likely smaller cells were able to move through the small pores consistently, which is why we observed an equal population of cells that jumped either once or more than once (Fig. 5C).

Discussion

We have systematically investigated the effects of scaffold pore diameter, matrix stiffness, and adhesivity as independently tunable parameters that govern marrow-derived stem cell motility. Initial intuition would guide anticipation that cells should migrate between void chambers most efficiently in scaffolds for which the pore diameter is the largest, as increasing pore diameter should presumably allow least hindered motility. However, this anticipated result was not borne out generally across the landscape of scaffold properties tested in our "inverse opal" constructs. Indeed, we were struck by the finding that maximal cell displacement into the scaffold was found in constructs possessing intermediate (12 μm) pore diameter at the stiffest and most adhesive conditions used in this study (Fig. 2B), and not in the larger and presumably non-restrictive 17 μm pore diameter (Fig. 2C). This novel and surprising phenomenon could be explained by the fact that, in the 12 μm pore diameter condition, cells are encountering pores more often than in the 17 μm pore diameter condition, due to the reduced void chamber diameter. However, this intuition is a bit unsatisfactory, given that in the largest void chambers the median speed of cells that never move through a pore is just under 20 μm/h.

Another potential explanation is that cells are able to sense a gradient in *structural* stiffness as they travel near pores. Since gels are made by sphere-templating, the hydrogel thins to a peak at the site of a pore, which will increase the structural compliance of that hydrogel region and thus may deform more significantly in response to cell traction forces. Seminal 2D migration work has shown that mesenchymal-type cells are able to sense and respond to hydrogel surface stiffnesses and, if presented with an interface, will preferentially migrate onto the stiffer substratum (Lo et al., 2000). Given this prior evidence, we thought it possible that cells were avoiding pore sites due to a possible stiffness gradient. While observing cells that migrated along the top of the macroporous gels, which contained many different areas of hydrogel thickness due to the templating process, we did not observe cells persisting on thicker areas of gel, making this potential durotaxis phenomenon in our scaffolds unlikely (Suppl. Mov. 2).

The largest pore diameters are most likely not restrictive to cell squeezing as the pore diameter (17 μm, Fig. 3F) approaches the spherical cell diameter (16 μm). Therefore, motility in this case is dominated by the cell traversing the sides of the void chamber, and cells in these scaffolds are often experiencing a quasi-2D environment, making their speed and path length most sensitive to changes in stiffness and adhesivity (Fig. 3C and Suppl. Fig. 2C). The most striking aspect of cell migration in this largest pore diameter case was the overall lack of interchamber movement in the presence of non-restrictive pore diameters. Instead, we observed a high population of cells in this case that underwent a sort of "hamster-wheeling" motility behavior within a singular void chamber (Suppl. Mov. 3). Unfortunately, due to competing effects of resolution requirements and cell photo-cytotoxicity, we were unable to clearly visualize live, migrating cells and pores simultaneously at high resolution. However, by qualitative observation of hundreds of cells (as shown in Suppl.

Mov. 3), it appeared that there was a tendency for cells to completely avoid pores and migrate along consistent ''tracks'' of material, rather than to locally search pores and then alter trajectories to avoid moving through them. This type of motility was able to generate high cell speeds and path lengths, yet did not result in large overall displacement. In the intermediate pore diameter case (12 μm pore, 40 μm void chamber), cells also did not jump often, but had a higher probability of jumping multiple times than cells in the largest pore diameter containing scaffolds (Fig. 5C).

This unexpected convolution between pore diameter and void chamber diameter has raised interesting questions about the true ''dimensionality'' a cell experiences in 3D microenvironements. In the smallest pore diameters, cells are experiencing a truly 3D environment, in that they are essentially entirely surrounded by the synthetic ECM. In this case, cell displacement, speed, and path length were all limited by restrictive pores and did not depend on matrix stiffness or adhesivity. In the opposite extreme, cells in the largest void chambers are more accurately in a quasi-2D environment, given that matrix space between pores is larger than the average cell width. This quasi-2D scenario was the only porous condition that led to cell speeds that were sensitive to changes in matrix adhesivity and stiffness (Fig. 3), which is interesting as previous work with implanted scaffolds in tibial wounds showed a biphasic relationship between osseous ingrowth and RGD functionalization (Eid et al., 2001). In the intermediate pore diameter case, cell width approached the diameter of matrix between pores, leading to increased jumping between pores (due to an increase in forced encounters with pores), yet no cell speed dependence on matrix stiffness and adhesivity.

These dimensionality arguments have concurrently emerged in work in 3D fibrillar gels, wherein the mode of matrix polymerization has profound affects on migratory phenotype (Harley et al., 2008; Kim et al., 2008; Doyle et al., 2009). Work by Kim et al. (2008) observed that glioblastoma cells were insensitive changes in 3D Type I Collagen gel stiffness or adhesivity, regardless of serum content. Interestingly, work by Harley et al. (2008) in Type I Collagen matrices that were formed using freeze-drying techniques found that motility was dependent on the stiffness of individual collagen fibers. This freeze-drying technique of matrix formation, however, created pore sizes that were in excess of 100 μm in diameter, so it is likely that cells in these matrices were experiencing a quasi-1D migratory microenvironment, rather than a 3D environment dominated by cell sampling of multiple pores and paths. Recent work by Doyle et al. (2009) has provided further insight concerning these matrix geometrical effects, where they used a 3D matrix also structurally dominated by long thin fibers. Using 2D PDMS model substrates and cell-derived 3D-like fibrous matrices, they found that cell speeds along PDMS lines (''1D mode'') mimicked speeds along matrix fibers (''3D mode''), and that both of these morphologies led to speeds that were much faster than cells on uniform 2D surfaces. Interestingly, motility along these 1D printed lines was only minimally influenced by alterations in adhesive protein density. In all those cases, as well as in the work presented here, it has been observed that matrix geometry may be a predominant biophysical cue and ultimately responsible for determining the phenotypic sensitivity to alterations of other biophysical factors (namely matrix stiffness and adhesivity).

Ideally, future studies would eliminate this dependence of pore diameter on void chamber size in order to parse out the pore diameter cue from these geometric phenomena. Unfortunately, attempts in our lab on sintering the templating beads to increase connectivity with smaller beads led to irreproducible pore diameters and other inconsistent material properties. A recent study attempting to deconvolute these parameters with polyacrylamide inverse opal gels showed some promise, though the annealing temperatures in that study showed an interdependence of pore diameter on the elastic modulus of the macroscopic scaffold (da Silva et al., 2010). As an alternative, interesting theoretical work may provide insight on combining beads of different sizes to potentially usurp this issue (Cottin and Monson, 1995).

Conclusions

Using a sphere-templating approach, we have created scaffolds with tunable stiffness, adhesivity, and porosity in which to study the migration of mesenchymal progenitor cell migration in model 3D scaffolds. Due to the convoluting parameters of void chamber diameter and pore diameter, interesting geometric relationships between cell width and the distance between available pores emerged. This geometric cue was the most powerful determinant of cell migratory phenotype observed here, and allowed for non-intuitive displacement behavior. Further, cells in a quasi-2D environment (large void chambers) were sensitive to local changes in matrix stiffness and adhesivity, while those in smaller chambers (more 3D-like environments) were not. These observations are interesting given other recent discoveries of the influence of matrix mechanics and adhesivity on cell migration on 2D environments and within 3D fibrillar matrices, and may lend insight to further developments in rational scaffold design for regenerative medicine.

The authors thank L. Stockdale and A. Bershteyn for technical assistance, and H. Lee, W. Kuhlman, and H.-D. Kim for helpful discussions. This work was generally supported by the NIGMS Cell Migration Consortium grant GM064346, with additional support to S. Peyton by NIGMS NRSA fellowship GM083472 and to K.J. Van Vliet by NSF CAREER CBET-0644846.

References

Canal T, Peppas NA. 1989. Correlation between mesh size and equilibrium degree of swelling of polymeric networks. J Biomed Mater Res 23(10):1183–1193.

Chen HC, Hu YC. 2006. Bioreactors for tissue engineering. Biotechnol Lett 28(18):1415–1423.
Constantinides G, Kalcioglu ZI, McFarland M, Smith JF, Van Vliet KJ. 2008. Probing mechanical properties of fully hydrated gels and biological tissues. J Biomech 41(15):3285–3289.
Cottin X, Monson PA. 1995. Substitutionally ordered solid-solutions of hard-spheres. J Chem Phys 102(8):3354–3360.
Cukierman E, Pankov R, Stevens DR, Yamada KM. 2001. Taking cell–matrix adhesions to the third dimension. Science 294(5547):1708–1712.
da Silva J, Lautenschlager F, Sivaniah E, Guck JR. 2010. The cavity-to-cavity migration of leukaemic cells through 3D honey-combed hydrogels with adjustable internal dimension and stiffness. Biomaterials 31(8):2201–2208.
Doyle AD, Wang FW, Matsumoto K, Yamada KM. 2009. One-dimensional topography underlies three-dimensional fibrillar cell migration. J Cell Biol 184(4):481–490.
Eid K, Chen E, Griffith L, Glowacki J. 2001. Effect of RGD coating on osteocompatibility of PLGA-polymer disks in a rat tibial wound. J Biomed Mater Res 57(2):224–231.
Engler AJ, Sen S, Sweeney HL, Discher DE. 2006. Matrix elasticity directs stem cell lineage specification. Cell 126(4):677–689.
Even-Ram S, Yamada KM. 2005. Cell migration in 3D matrix. Curr Opin Cell Biol 17(5):524–532.
Flory PJ. 1953. Principles of polymer chemistry. Ithaca, NY: Cornell University Press. p. 688.
Friedenstein AJ, Piatetzky S II, Petrakova KV. 1966. Osteogenesis in transplants of bone marrow cells. J Embryol Exp Morphol 16(3):381–390.
Gibson LJ, Ashby M. 1999. Cellular solids: Structure and properties. New York, NY: Cambridge University Press. p. 532.
Harley BA, Leung JH, Silva EC, Gibson LJ. 2007. Mechanical characterization of collagen-glycosaminoglycan scaffolds. Acta Biomater 3(4):463–474.
Harley BA, Kim HD, Zaman MH, Yannas IV, Lauffenburger DA, Gibson LJ. 2008. Microarchitecture of three-dimensional scaffolds influences cell migration behavior via junction interactions. Biophys J 95(8):4013–4024.
Healy KE, Guldberg RE. 2007. Bone tissue engineering. J Musculoskelet Neuronal Interact 7(4):328–330.
Jain A, Rogojevic S, Gill WN, Plawsky JL, Matthew I, Tomozawa M, Simonyi E. 2001. Effects of processing history on the modulus of silica xerogel films. J Appl Phys 90(11):5832–5834.
Jiang Y, Jahagirdar BN, Reinhardt RL, Schwartz RE, Keene CD, Ortiz-Gonzalez XR, Reyes M, Lenvik T, Lund T, Blackstad M, Du J, Aldrich S, Lisberg A, Low WC, Largaespada DA, Verfaillie CM. 2002. Pluripotency of mesenchymal stem cells derived from adult marrow. Nature 418(6893):41–49.
Jing Y, Mal N, Williams PS, Mayorga M, Penn MS, Chalmers JJ, Zborowski M. 2008. Quantitative intracellular magnetic nanoparticle uptake measured by live cell magnetophoresis. FASEB J 22(12):4239–4247.
Kasten P, Beyen I, Niemeyer P, Luginbuhl R, Bohner M, Richter W. 2008. Porosity and pore size of beta-tricalcium phosphate scaffold can influence protein production and osteogenic differentiation of human mesenchymal stem cells: An in vitro and in vivo study. Acta Biomater 4(6):1904–1915.
Kim HD, Guo TW, Wu AP, Wells A, Gertler FB, Lauffenburger DA. 2008. Epidermal growth factor-induced enhancement of glioblastoma cell migration in 3D arises from an intrinsic increase in speed but an extrinsic matrix- and proteolysis-dependent increase in persistence. Mol Biol Cell 19(10):4249–4259.
Kobune M, Kawano Y, Ito Y, Chiba H, Nakamura K, Tsuda H, Sasaki K, Dehari H, Uchida H, Honmou O, Takahashi S, Bizen A, Takimoto R, Matsunaga T, Kato J, Kato K, Houkin K, Niitsu Y, Hamada H. 2003. Telomerized human multipotent mesenchymal cells can differentiate into hematopoietic and cobblestone area-supporting cells. Exp Hematol 31(8):715–722.
Kumagai K, Vasanji A, Drazba JA, Butler RS, Muschler GF. 2008. Circulating cells with osteogenic potential are physiologically mobilized into the fracture healing site in the parabiotic mice model. J Orthop Res 26(2):165–175.
Kundu AK, Putnam AJ. 2006. Vitronectin and collagen I differentially regulate osteogenesis in mesenchymal stem cells. Biochem Biophys Res Commun 347(1):347–357.
Lee JY, Choo JE, Choi YS, Shim IK, Lee SJ, Seol YJ, Chung CP, Park YJ. 2009. Effect of immobilized cell-binding peptides on chitosan membranes for osteoblastic differentiation of mesenchymal stem cells. Biotechnol Appl Biochem 52(Pt 1):69–77.
Lo CM, Wang HB, Dembo M, Wang YL. 2000. Cell movement is guided by the rigidity of the substrate. Biophys J 79(1):144–152.
Maheshwari G, Wells A, Griffith LG, Lauffenburger DA. 1999. Biophysical integration of effects of epidermal growth factor and fibronectin on fibroblast migration. Biophys J 76(5):2814–2823.
Maheshwari G, Brown G, Lauffenburger DA, Wells A, Griffith LG. 2000. Cell adhesion and motility depend on nanoscale RGD clustering. J Cell Sci 113(Pt 10):1677–1686.
Maloney JM, Nikova D, Lautenschlager F, Clarke E, Langer R, Guck J, Van Vliet KJ. 2011. Mesenchymal stem cell mechanics from the attached to the suspended state. Biophys J 99(8): 2479–2487.
Marshall AJ, Ratner BD. 2005. Quantitative characterization of sphere-templated porous biomaterials. AIChE J 51(4):1221–1232.
Martino MM, Mochizuki M, Rothenfluh DA, Rempel SA, Hubbell JA, Barker TH. 2009. Controlling integrin specificity and stem cell differentiation in 2D and 3D environments through regulation of fibronectin domain stability. Biomaterials 30(6):1089–1097.
Ochsner M, Textor M, Vogel V, Smith ML. 2010. Dimensionality controls cytoskeleton assembly and metabolism of fibroblast cells in response to rigidity and shape. PLoS ONE 5(3):e9445.
Okamoto T, Aoyama T, Nakayama T, Nakamata T, Hosaka T, Nishijo K, Nakamura T, Kiyono T, Toguchida J. 2002. Clonal heterogeneity in differentiation potential of immortalized human mesenchymal stem cells. Biochem Biophys Res Commun 295(2):354–361.
Oliver WC, Pharr GM. 1992. An improved technique for determining hardness and elastic-modulus using load and displacement sensing indentation experiments. J Mater Res 7(6):1564–1583.
Palecek SP, Loftus JC, Ginsberg MH, Lauffenburger DA, Horwitz AF. 1997. Integrin-ligand binding properties govern cell migration speed through cell-substratum adhesiveness. Nature 385(6616):537–540.
Peyton SR, Putnam AJ. 2005. Extracellular matrix rigidity governs smooth muscle cell motility in a biphasic fashion. J Cell Physiol 204(1):198–209.
Peyton SR, Ghajar CM, Khatiwala CB, Putnam AJ. 2007. The emergence of ECM mechanics and cytoskeletal tension as important regulators of cell function. Cell Biochem Biophys 47(2):300–320.
Pittenger MF, Mackay AM, Beck SC, Jaiswal RK, Douglas R, Mosca JD, Moorman MA, Simonetti DW, Craig S, Marshak DR. 1999. Multilineage potential of adult human mesenchymal stem cells. Science 284(5411):143–147.
Roh JD, Nelson GN, Udelsman BV, Brennan MP, Lockhart B, Fong PM, Lopez-Soler RI, Saltzman WM, Breuer CK. 2007. Centrifugal seeding increases seeding efficiency and cellular distribution of bone marrow stromal cells in porous biodegradable scaffolds. Tissue Eng 13(11):2743–2749.
Sanz-Herrera JA, Moreo P, Garcia-Aznar JM, Doblare M. 2009. On the effect of substrate curvature on cell mechanics. Biomaterials 30(34):6674–6686.
Sekiya I, Larson BL, Smith JR, Pochampally R, Cui JG, Prockop DJ. 2002. Expansion of human adult stem cells from bone marrow stroma: Conditions that maximize the yields of early progenitors and evaluate their quality. Stem Cells 20(6):530–541.
Shegarfi H, Reikeras O. 2009. Review article: Bone transplantation and immune response. J Orthop Surg (Hong Kong) 17(2):206–211.
Simmons CA, Matlis S, Thornton AJ, Chen S, Wang CY, Mooney DJ. 2003. Cyclic strain enhances matrix mineralization by adult human mesenchymal stem cells via the extracellular signal-regulated kinase (ERK1/2) signaling pathway. J Biomech 36(8):1087–1096.

Smith KE, Hyzy SL, Sunwoo M, Gall KA, Schwartz Z, Boyan BD. 2010. The dependence of MG63 osteoblast responses to (meth)acrylate-based networks on chemical structure and stiffness. Biomaterials 31(24):6131–6141.

Stachowiak AN, Irvine DJ. 2008. Inverse opal hydrogel-collagen composite scaffolds as a supportive microenvironment for immune cell migration. J Biomed Mater Res A 85(3):815–828.

Stachowiak AN, Bershteyn A, Tzatzalos E, Irvine DJ. 2005. Bioactive hydrogels with an ordered cellular structure combine interconnected macroporosity and robust mechanical properties. Adv Mater 17(4):399–403.

Sumanasinghe RD, Bernacki SH, Loboa EG. 2006. Osteogenic differentiation of human mesenchymal stem cells in collagen matrices: Effect of uniaxial cyclic tensile strain on bone morphogenetic protein (BMP-2) mRNA expression. Tissue Eng 12(12):3459–3465.

Thompson MT, Berg MC, Tobias IS, Rubner MF, Van Vliet KJ. 2005. Tuning compliance of nanoscale polyelectrolyte multilayers to modulate cell adhesion. Biomaterials 26(34):6836–6845.

Tugulu S, Arnold A, Sielaff I, Johnsson K, Klok HA. 2005. Protein-functionalized polymer brushes. Biomacromolecules 6(3):1602–1607.

Tugulu S, Silacci P, Stergiopulos N, Klok HA. 2007. RGD—Functionalized polymer brushes as substrates for the integrin specific adhesion of human umbilical vein endothelial cells. Biomaterials 28(16):2536–2546.

Zaman MH, Kamm RD, Matsudaira P, Lauffenburger DA. 2005. Computational model for cell migration in three-dimensional matrices. Biophys J 89(2):1389–1397.

Zaman MH, Trapani LM, Siemeski A, Mackellar D, Gong H, Kamm RD, Wells A, Lauffenburger DA, Matsudaira P. 2006. Migration of tumor cells in 3D matrices is governed by matrix stiffness along with cell–matrix adhesion and proteolysis. Proc Natl Acad Sci USA 103(29):10889–10894.